

Inverse Design of Inorganic Electrides

Yunwei Zhang¹, Hui Wang¹, Yanchao Wang¹, Lijun Zhang¹, and Yanming Ma^{1,*}

¹*State Key Lab of Superhard Materials, Jilin University, Changchun 130012, China*

*Address correspondence to: mym@calypso.cn

Electrides are ionic solids that consist of cationic frameworks and anionic electrons trapped in the voids of lattices. Organic electrides exist in a large abundance, but the thermal instability at room temperature and sensitivity to moisture are bottlenecks that limit their practical uses. Known inorganic electrides are rare but appear to have high thermal and chemical stability and exhibit promising applications as electron-emitting materials, superior catalysts and strong reducing agents. Here, we report a developed inverse-design method that can be used to search for a large variety of inorganic electrides. Our method utilizes the intrinsic property of interstitial electron localization of electrides as the global variable function being incorporated into the swarm-intelligence based structure searches. Through screening 99 binary ionic compounds, we have designed 89 new inorganic electrides that are classified into three-, two-, and zero-dimensional species according to the way that the interstitial electrons are localized and the conductive properties of the systems. Our work reveals the rich abundance of inorganic electrides by extending them into more general forms and provides new structure types for electrides that are not thought of as before.

Electrides are ionic solids with excess electrons trapped at the interstitial areas of lattices, which serve as anions¹⁻². The strongly or loosely localized electrons make electrides relate to salts with F-centers or plasmas, but markedly differ from metals containing delocalized electrons³. So far, most of the synthesized electrides are organic species composed of alkali metals ions complexed with crown ethers for the cations. The solvent electrons released by alkali metals are trapped in potential wells formed between these complexed cations^{3,4,5,6}. Though they are reported as low-temperature electron emitters and strong reducing materials^{4,5,7}, the thermal instability above -40°C and sensitivity to air and water restrict their practical application.

The first inorganic electride C12A7:e was synthesized in 2003 by removing oxygen ions from the center of the clathrate Ca-Al-O cages of mayenite (12CaO₇·Al₂O₃)⁸. It shows superior properties that are thermally stable at room temperature and chemically stable in resisting to water and air. Excellent field-emission property is evident with even lower work function than carbon nanotubes⁹. An order of magnitude higher catalytic property than standard ones (such as iron-based catalyst Fe-Al₂O₃-K₂O¹⁰) is manifested when loading on Ru element in the ammonia synthesis¹¹.

Dicalcium nitride (Ca₂N) was recently proved to be a two-dimensional (2D) electride where anionic electrons are weakly localized in the 2D interspaces between two positively charged ionic [Ca₂N]⁺ layers¹². Ca₂N was then used as an efficient electron donating agent in the transfer hydrogenation of alkynes and alkenes¹³. Monolayer Ca₂N encapsulated by graphene shows excellent predicted electron transport properties if compared to typical 2D electronic systems (e.g., GaAs-AlGaAs heterojunction, LaAlO₃-SrTiO₃ interface and graphene)¹⁴.

As an important category of inorganic electrides,

high-pressure electrides were predicted in various simple elemental metals^{15,16,17,18,19}. These elemental electrides are unique and differ from electron-rich ionic electrides seen at ambient pressure²⁰. A drawback is that these high-pressure electrides are not quenchable to ambient conditions and hardly to be of any practical use.

Recently, a substitutional screening method²¹ has been applied to search for 2D electrides. The rhombohedral anti-CdCl₂-type structure of Ca₂N was used as a prototype electride structure where Ca and N were replaced with alternative metal elements (e.g., alkali and transition metals) and non-metal elements (e.g., halogen elements, O and C), respectively. On the one hand, the method is successful, especially when the potential electrides do crystallize in the same structure. There is the case on the prediction of Y₂C electride that led to the actual experimental observation²². On the other hand, this method fails since it confines electrides in a certain structure type, which, however, limits our understanding of the diversity of electride structures. The predicted electrides strongly rely on the known structure types, while a finding of electrides with an unknown structure is impossible.

As described above, the inorganic electrides at ambient conditions are rarely known. This inevitably limits the wide range of applications of electrides. A massive computation-assisted design of inorganic electrides is highly desirable. Here we developed an efficient inverse-design method that relies on the intrinsic physical property of interstitial electron localization other than any prior known electride structures to search for a variety of new inorganic electrides. Our method has been incorporated into our in-house developed CALYPSO structure prediction code^{23,24,25} enabling automatic structure searches through intelligent exploration of various unknown structure types. Our method is reliable to identify the known electrides of Ca₂N¹² and high pressure

transparent Na^{15} with the only given information of chemical compositions. Extensive inverse-design simulations on 99-targeted binary ionic systems were then performed, and 89 new electrides were successfully designed, some of which have already been synthesized, though not yet being pointed out as electrides, while others are new compounds awaiting experimental synthesis. We unraveled rich abundance of inorganic electrides by extending them into more general forms. A large variety of new prototype structures for electrides that are not thought of as before were reported.

Results and Discussion

Inverse-Design Methodology. Our inverse-design method is on top of our developed swarm-intelligence based CALYPSO structure searching method that is able to intelligently explore structures with the only given information on chemical composition for a compound without relying on any prior known structural information²⁴. In the current implementation, the degree of interstitial electron localization other than the total energy was introduced and adopted as the global variable function. This is in good accordance with the fact that strong electron localization in the voids of lattice is the intrinsic physical property of electrides. Our structural design follows the principle of inverse design where the structure searches are forced into a pursuit of a structure having a desirable functionality for a given chemical system. Our previous inverse-design exercise has been applied into the searching of superhard materials²⁶.

As a powerful technique to identify core, binding, and lone-pair regions in chemical systems, electron localization function (ELF)^{27,28,29} provides a semi-quantitative index for the measure of interstitial electron localization. We define the degree of interstitial electron localization as the indicator to characterize the interstitially localized electrons. The indicator adopts the formula of $\omega = V_{\text{inter}}/V_{\text{cry}}$, where V_{inter} and V_{cry} are the volumes of the interstitial regions where electrons localize well and the simulation cell, respectively. V_{inter} is critically determined from the reliable ELF calculation. A detailed description on how to obtain a precise interstitial V_{inter} can be found in Supplementary Table S1 and Fig. S1. A larger ω gives a higher probability of the formation of electrides in a crystal. Though choices of ELF values for characterizing electron localization are dependent of specific systems, in our test, we found that ELF values larger than 0.75 can give a good description for electron localization for most of systems.

Our inverse-design approach is outlined in Fig.1a. In the first generation, all structures are generated randomly with the symmetry constraints. Structures are then geometrically optimized for seeking for their local minima in the potential surface. ω values of optimized structures are evaluated to rank good electride structures. A certain number of structures (here we chose 60% of the population size) with high- ω values are evolved into next generation by swarm-optimization operation via a smart learning of personal and global best electride structures²³³⁰. The rest 40% structures in each generation are randomly generated to enhance structural diversity during the structure evolution.

Eventually, we are able to construct ω vs. energy map in an effort to trace the generated structures for acquiring desired electrides (e.g., Fig. 1b).

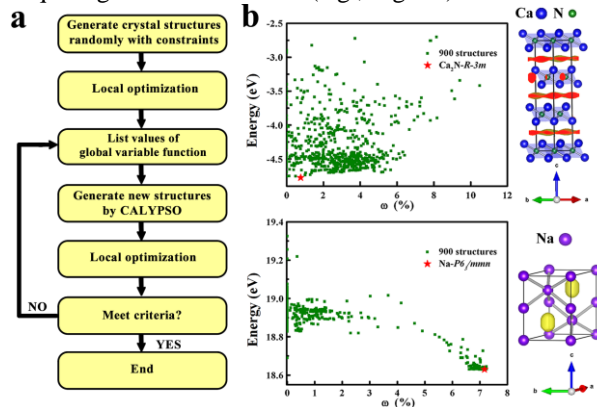


Figure 1. Inverse-design scheme for electrides and its benchmarks on two known electrides of Ca_2N and transparent Na at 320 GPa. (a) Flow chart of CALYPSO module for searching for electrides by the inverse-design scheme. (b) ω vs. energy maps of Ca_2N at ambient pressure (top left panel) and elemental sodium at 320 GPa (bottom left panel). Green squares represent structures produced by CALYPSO run within 30 generations. The experimental anti- CdCl_2 and hP4 electride structures for Ca_2N and sodium are shown as red stars in left panels and depicted in top and bottom right panels, respectively.

Benchmarks on Known Electrides. We have benchmarked our inverse-design method onto two known electride systems: Ca_2N (and its variants, such as Sr_2N and Y_2C , shown in Supplementary Fig. S2) at ambient pressure and high-pressure electride of transparent sodium at 320 GPa. With the only input information of chemical compositions of $\text{Ca}:\text{N} = 2:1$, our calculations readily reproduced the experimental electride anti- CdCl_2 -type structure of Ca_2N as seen in Fig. 1b (top right panel) via the calculated ω vs. energy map (top left panel of Fig. 1b). Our calculations also correctly reproduced the hP4 electride structure (bottom right panel of Fig. 1b) of sodium at 320 GPa as seen in the calculated ω vs. energy map of Fig 1b (bottom left panel). This certifies the validity of our method in application to design of high-pressure electrides. Note that the valence electrons of sodium at 320 GPa are completely localized in the voids of hP4 structure that leads to the formation of an insulating electride¹⁵.

Two Design Principles for Inorganic Electrides. It is known that electrides, such as $[\text{Ca}_{24}\text{Al}_{28}\text{O}_{64}]^{4+}$ ($4e^-$) and $[\text{M}_2\text{N}]^+$ (e^-) ($\text{M} = \text{Ca}, \text{Sr}$ and Ba), contain intrinsic excess of electrons. Existence of excess electrons in a chemical system should be regarded as a necessary condition for stabilizing an electride and therefore has been used as one of our design principles in searching for inorganic electrides. We further prove this design principle in a model system by removing one excess electron per formula unit of Ca_2N . Upon depletion of its excess electron Ca_2N is not an electride any more without showing any electron localization between the positively charged $[\text{Ca}_2\text{N}]^+$ layers (shown in Fig. 2a). In below context, we define the electron-rich binary systems into a general form of $[\text{A}_x\text{B}_y]^{n+}$ (ne^-) (x, y and n are integers; A and B are cationic and anionic elements as electrons donor and acceptor, respectively)

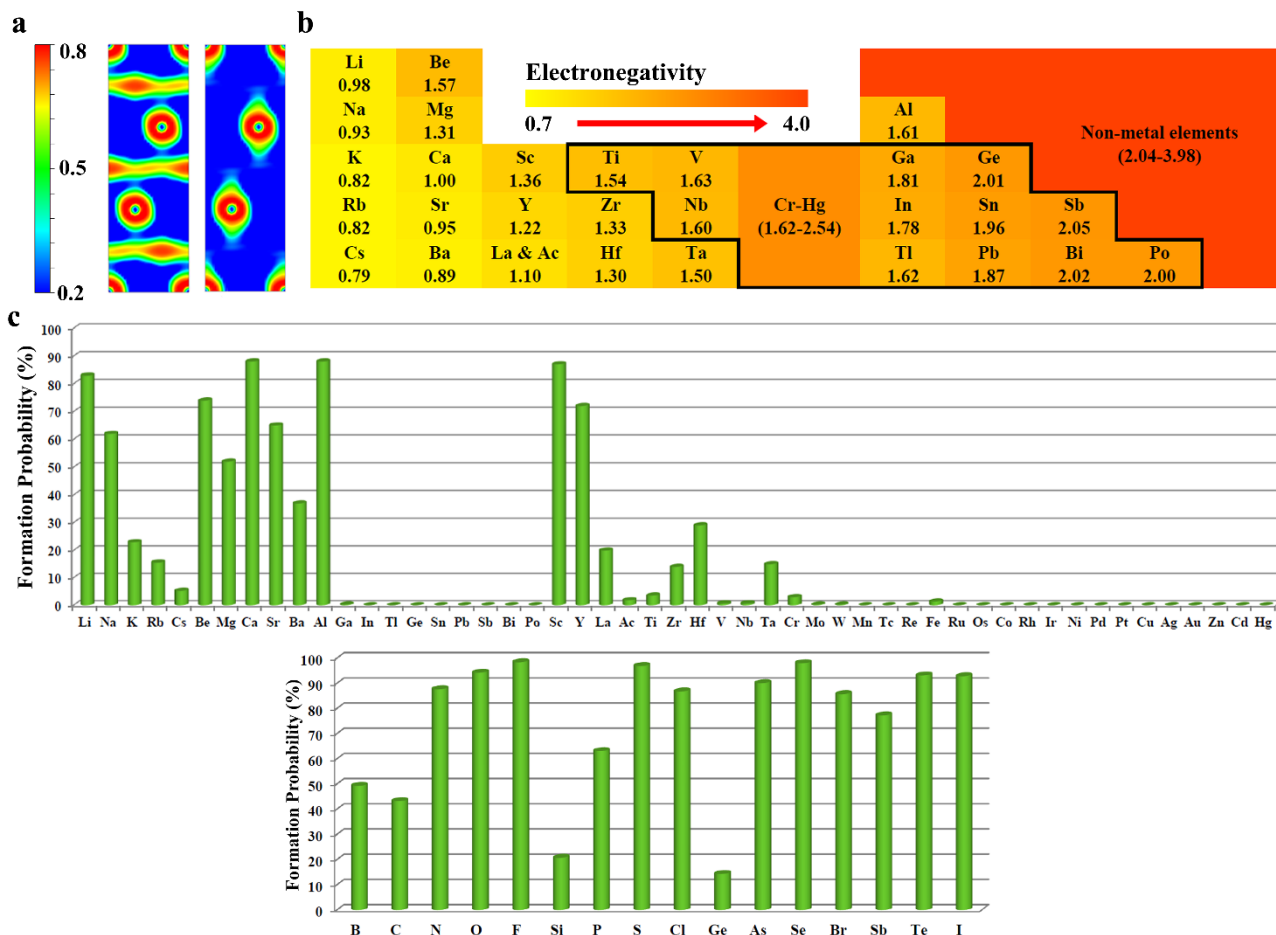


Figure 2 | Tests for two design principles. (a) The electron localization function of Ca_2N (left panel) on the $(110)_R$ plane parallel to the hexagonal c -axis. Upon removal of one excess electron per Ca_2N , the system loses the feature of electron localization (right panel). (b) Electronegativity of elements by Pauling scale³¹. Metallic elements with higher electronegativity than Be are not good electron donors for binary electrides. (c) The formation probabilities (ratios of electride phases over all generated structures by CALYPSO code) of electrides in metal nitrides and Ca_2X compounds are plotted in top and bottom panels, respectively. Metal and X elements are listed along x axis and formation probabilities of each compounds are shown as y axis.

for searching for potential electrides. These electron-rich ionic systems are in contrast to those conventional ionic solids (e.g., Ca_3N_2 , YN and NaCl, etc.) that follow the rule of electroneutrality where the sum of the formal charges of all constituent elements is equal to zero.

Electronegativity of elements is another critical principle for the design of electrides since it is a direct measure of an element's ability to attract or donate electrons. We choose metal nitrides (La and Ac are representatives of lanthanides and actinides, respectively) and Ca_2X (X = nonmetallic elements or metallic elements with high electronegativity comparable to nonmetals, such as Ge, Sb and Bi) as two model systems to illustrate how electronegativities of cationic and anionic elements can influence the formation of electrides in certain systems. Metal nitrides containing excess electrons, such as $[\text{M}_4\text{N}]^+ e^-$ for alkali metal nitrides and $[\text{M}_2\text{N}]^+ e^-$ for alkaline earth metal nitrides are examined (the results on other metal nitrides are listed in Supplementary Table S3). The formation probability of electrides, *i.e.*, the ratio of the generated electride structures over all structures produced by our inverse-design simulations, is plotted out in Fig. 2c. We found that only those metallic

elements with low electronegativity are preferable to the formation of electrides. Specifically, nitrides formed by metallic elements in IA, IIA, and IIB groups and aluminum have higher formation probabilities of electrides, while the probabilities are much lower for IVB (e.g., Zr and Hf) elements. A few electrides in Ti and V nitrides appear, but they are energetically too unfavorable to allow the experimental synthesis. Other metallic elements having even higher electronegativity (indicated in the bold black frame in Fig. 2b) cannot form any electride phases.

For the Ca_2X systems, we found most of testing objects have high formation probability of electrides beyond 50% (bottom panel in Fig. 2c), except for Ca_2B and $\text{Ca}_2\text{-IVA}$ compounds (e.g., Ca_2C , Ca_2Si and Ca_2Ge). These latter four systems are not intrinsic electron-rich compounds through intuitive calculation of the sum of the formal charges of constituent elements. Most of the generated structures are therefore not electrides. Electride structures appear only when the anionic elements form pairs in the structure. Once paired, the resultant structure becomes an electron-rich system containing excess electrons satisfying the requirement for the formation of electride. Comparing the model calculation results of Ca_2X system with those of metal

nitrides, we found that the choice of cationic elements (other than the anionic elements) has a critical effect on the formation of electrides. Hence, it is desirable to

confine our searching of electrides into those electron-rich systems composed of cationic elements with low electronegativity.

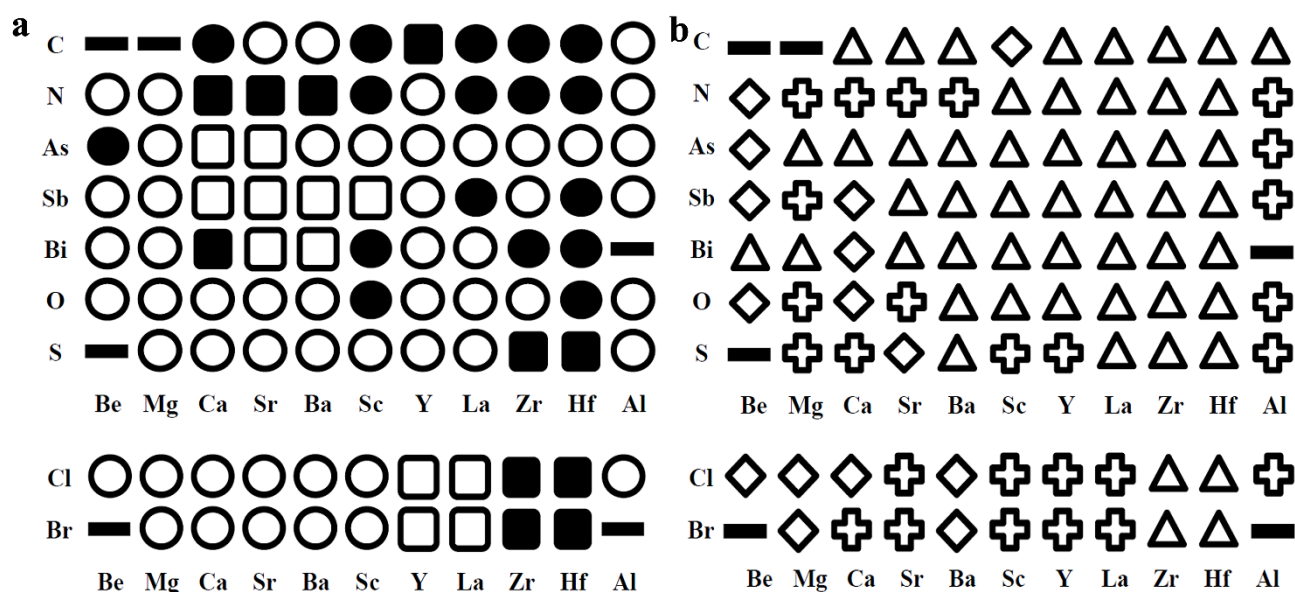


Figure 3 | Inverse-design results of binary electrides. (a) Stability Map of A₂B (top) and AB (bottom) (A = electrons donor, B = electrons acceptor) electrides. Black lines indicate the absence of any reasonable electride phase in that system. Squares and circles denote the predicted electrides are existing compounds and yet to be synthesized, respectively. Solid symbols indicate the energetically stable phases (have negative formation energies) with respect to the existing compounds, while open symbols for metastable phases (have positive formation energies). (b) Type Map of A₂B (top) and AB (bottom) electrides: triangles for 3D, diamonds for 0D, and crosses for 2D. Black lines indicate the same as in (a).

New Electrides by Inverse-Design Simulations. We conducted extensive inverse-design simulations through CALYPSO code on 99 electron-rich A₂B and AB systems composed of 11 cationic A elements with low electronegativity playing the role of electron donors and 9 anionic B elements (7 non-metallic elements and 2 metallic elements with high electronegativity) as electron acceptors as shown in Fig. 3. Our calculations readily reproduced the correct anti-CdCl₂ structure shared by four known Ca₂N, Sr₂N, Ba₂N and Y₂C electrides^{1,12,22}. We ruled out the formation possibility of electrides in nitrides and carbides dominating the hexagonal structure.

We here reported 89 newly designed electrides as depicted in the Stability Map (Fig. 3a). 3D ELF maps, structure information and formation energies of these electrides are shown in Supplementary Table S2. It is noted that for one particular system, many electride structures are generated in our simulation, however; only the electride having the lowest-energy structure has been presented in Fig. 3a. Among these 89 electrides, 19 are existing compounds (square symbols in Fig. 3a), but yet to be pointed out as electrides. The other 70 electrides (circle symbols in Fig. 3a) are hitherto unknown compounds awaiting experimental synthesis: 17 electrides are energetically stable (i.e., having negative formation energies) shown as solid circles in Fig. 3a, while the other 53 are metastable (i.e., having positive formation energies) shown as open circles. It is noteworthy that our target systems contain intrinsic excess electrons and therefore go against the electroneutrality for acquiring stable compounds.

Chemically, this explains that some of our designed electrides are energetically metastable. In reality, these metastable electrides are experimentally synthesizable as seen in many examples on actual experimental syntheses (e.g., metastable compounds denoted by open squares in Fig.3a).

According to the way the excess electrons are localized and the conductive properties of systems, these electrides can be classified into three categories: 3D, 2D and 0D species as shown in Type Map (Fig. 3b), marked by different symbols. There are 52 3D, 22 2D, and 15 0D inorganic electrides, respectively. Below, we selected three compounds of Ca₂C, Be₂N and LaCl as the illustrative examples for 3D, 0D and 2D electrides, respectively, to discuss their structural and electronic properties.

Structures and Electronic Properties of Designed Electrides.

3D Electrides. In 3D electrides (shown as triangles in Fig. 3b), excess electrons are partially localized in the cavity interstitials of the lattice. There is a subtle balance between localization and delocalization of excess electrons that contribute to the conductivity in three dimensions. Ca₂C is a typical 3D electride that has a body-centered tetragonal *I4/mmm* structure (right panel in Fig. 4a) consisting of cationic Ca²⁺ and anionic C₂²⁻. This structure is a new prototype structure of electride that doesn't follow any known structures in the databases,^{32,33} and it can be derived from the insulating calcium dicarbide CaC₂³⁴ (left panel in Fig. 4a) by

replacing the dashed C_2 dimers with the interstitially localized electrons.

ELF results (right panel in Fig. 4b) showed that excess electrons are partially localized in anionic cavity sites that are linked each other by delocalized electrons. The calculated partial electron density for region near Fermi level (right panel in Fig. 4c) illustrates that these delocalized electrons dominate the conductivity of Ca_2C . The 3D conducting behavior of excess electrons can also be inferred from the band structure of Ca_2C (left panel in Fig. 4c) at Fermi level that crosses over high symmetric directions along Z-A, A-M and X- Γ .

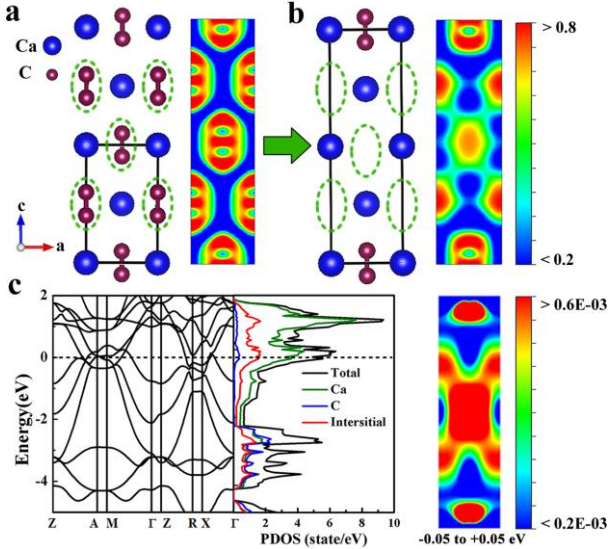


Figure 4 | Structural and electronic properties of Ca_2C and CaC_2 . (a) Crystal structure (left panel) and ELF (right panel) on $(0\bar{1}2)$ plane of CaC_2 . (b) Crystal structure (left panel) and ELF (right panel) on (012) plane of Ca_2C . Interstitial regions marked by dashed circles are where excess electrons localize. (c) Electronic properties of Ca_2C : band structure and PDOS (left panel), and partial electron density for region near E_F ($|E| < 0.05$ eV) on the (012) plane (right panel).

0D Electrides. Electron localization of 0D electrides (shown as diamonds in Fig. 3b) is geometrically similar to that of 3D electrides. However, excess electrons in 0D electrides are entirely localized and do not contribute to the conductivity. As a result, these 0D electrides show typically semiconducting/insulating behaviors, which are similar to some of known high-pressure electrides, such as hP4 sodium at 320 GPa¹⁵ and semiconducting Aba2-40 lithium at 70 GPa¹⁶.

Be_2N adopts an $R3m$ rhombohedral structure, a new electride structure that is also out of the known structure database^{32,33}. There are two kinds of N atoms in Be_2N : (i) in the first kind, N atoms are six-fold coordinated with Be atoms forming faces shared octahedrons along x-y plane; (ii) N atoms in the second kind are five-fold coordinated with Be atoms forming N centralized hexahedrons (left panel in Fig. 5a). Each hexahedron links to its neighboring hexahedrons or octahedrons by sharing one Be atom. ELF results (Fig. 5a) showed that excess electrons are entirely localized at empty crystallographic positions (yellow spheres in Fig. 5a) in the interstitials. The localized electrons in areas are discrete, which leads to the semi-conductivity of the system (as shown in its band structure in Fig. 5c).

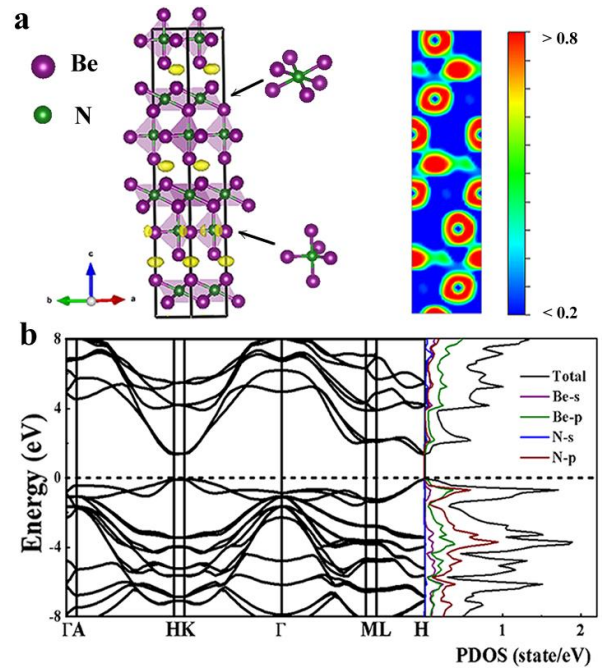


Figure 5 | Semiconducting Be_2N as a 0D electride. (a) 3D ELF of Be_2N (left panel) with an isosurface value of 0.83. Six-fold and five-fold coordinated Be atoms are pointed out as inset structural units in the left panel. 2D ELF on (110) plane is plotted out in right panel to show the isolated interstitial localization regions. (b) Band structure and partial density of states (PDOS) of Be_2N . The use of HSE06 functional^{35,36} corrects the DFT bandgap of 1.51 eV to 1.96 eV. Dashed line indicates the Fermi energy (E_F).

2D Electrides. In 2D electrides (shown as crosses in Fig. 3b), the excess electrons are confined within interspaces between cationic layers and contribute to the anisotropic conductivity of the system. Note that localized electrons in 2D electrides are not evenly distributed and there are non-nuclear electron maxima at crystallographic positions. 2D electrides have commonly layered structures, however, not all of layered electrides could fall into this category. For example, though Sc_2N and Y_2N share the same layered structure with that of Ca_2N , they are not regarded as 2D electrides since the excess electrons are localized so well at the interstitial crystallographic sites and do not contribute to the conductivity.

$LaCl$ ³⁷ adopts a layered $R-3m$ structure where atomic packing is arranged in a sequence of ABCBA (A, B and C are Cl^- sheets, La^{3+} sheets, and anionic electron layers, respectively) (Fig. 6a). Both La and Cl atoms form a graphene-like arrangement in their respective sheets.

ELF results (top panel in Fig. 6b) showed that the excess electrons are confined in the interlayer interstitial spacings between two La sheets, highlighted in a white dashed circle. Three centers of the maximally localized regions are arrayed into one group that connects each other throughout the layer by delocalized electrons. It is interesting to note that the conducting behaviors of the three centered excess electrons within one group are different. Partial electron density for region near Fermi level indicates that the excess electrons at both ends of one group (circled by a dashed white line in bottom panel in Fig. 6b) are partially localized and contribute to the conductivity of the system, however the excess electrons at the center of

the group are well localized without showing any conducting behavior. The dispersive band near Fermi level highlighted in red in band structure (left panel in Fig. 6c) is mainly occupied by interstitial electrons as illustrated by the density of state (right panel in Fig. 6c). The high symmetric lines of Γ -M-K- Γ and A-L-H-A in the reciprocal space depicted in Fig. 6d are indicative of 2D planes of the structure in real space where electrons are localized. The red bands cross Fermi level only along these symmetric lines, showing a clear 2D anisotropic conducting behavior of the system.

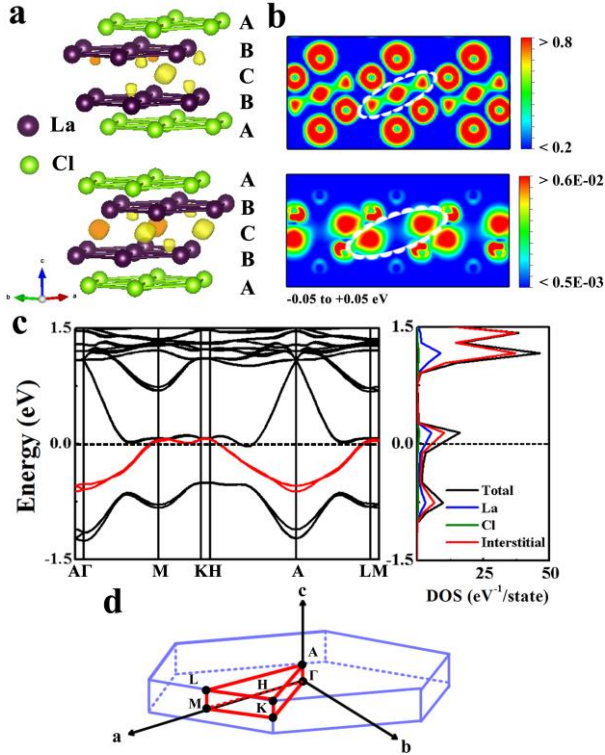


Figure 6 | Structural and electronic properties of LaCl. (a) 3D ELF of LaCl with an isosurface value of 0.7. (b) 2D ELF (top panel) on $(\bar{1}\bar{1}0)$ plane and partial electron density for region near E_F ($|E| < 0.05$ eV) (bottom panel) on the $(\bar{1}\bar{1}0)$ plane. (c) Band structure and electron density of state of LaCl. Plotting details are the same as in Figure 5. (d) The high symmetry lines (in red color) in the first Brillouin zone.

Conclusions

Our developed inverse-design method benefits from the swarm-intelligence based structure search that is able to generate hitherto unknown structure types, and therefore the method is in sharp contrast to the substitution method relying on the known electrider structure of anti- CdCl_2 one. We are able to reveal a rich variety of prototype structures of inorganic electrideres. 16 structural types out of 89 newly designed electrideres are even found to go beyond the known structure databases^{32,33} (detailed information for new prototype structures is listed in Supplementary Table S4).

We have extended electrideres into more general forms (such as $[\text{A}_x\text{B}_y]^{n+}(\text{ne})^n$ for binary systems) by considering the formal charges of constitute elements. The two choices of stoichiometry A_2B and AB are just two representative cases. In reality, there exist many alternative stoichiometries as candidates for electrideres not only in other binary compounds, but also in ternary, quaternary, and even more complex compounds that are ready for exploration. We believe the findings of electrideres will become a general activity especially with

the use of our developed inverse-design method. This is in sharp contrast to the current situation of the rarely known inorganic electrideres and the greatly limited practical application of inorganic electrideres.

Electron-rich ionic systems are chosen in our simulations. This doesn't exclude the possibility on the findings of electrideres whose stoichiometry follow the principle of electroneutrality, which is out of scope in this study. We found that electrideres can even be extended into electroneutral systems once specific chemical bondings are formed. For example, Ca_2C has been placed into an electrider system when C atoms form pairs.

In view of the observed superconductivity in the heavily electron-doped mayenite^{38,39}, we expect some of our predicted conducting electrideres might also show the similar superconducting property. Through explicit calculations of electron-phonon interaction, we found that 3D electrideres have potential to be superconducting though with low estimated T_c (e.g., 5 K for Ca_2Bi and 4.17 K for Sc_2As). The localized excess electrons can play an important role in the superconductivity of these compounds, which need a further study on the mechanism.

Methods

Structure prediction. Our structure searching simulations are performed through the swarm-intelligence based CALYPSO method^{23,24} enabling a global minimization of energy surfaces merging *ab initio* total-energy calculations as implemented in the CALYPSO code. The method has been benchmarked on various known systems. Here, the degree of interstitial electron localization was introduced as the fitness function in the search of electrider materials.

First-principles calculations. All the electronic structure calculations were performed using density functional theory within the Perdew-Burke-Ernzerhof of generalized gradient approximation as implemented in the Vienna Ab initio Simulation Package (VASP)⁴⁰. The projector-augmented wave (PAW)⁴¹ method was adopted with the PAW potentials taken from the VASP library. The HSE06 hybrid functional^{35,36} reproduces well the band gap of semiconductors, thus the HSE06 hybrid functional was applied to revise the band gaps⁴² of those semiconducting phases of zero-D electrideres calculated by the PBE functional. The plane-wave kinetic energy cutoffs of 800 eV and Monkhorst-Pack Brillouin zone sampling grid with the resolution of $2\pi \times 0.03 \text{ \AA}^{-1}$ were chosen to ensure that all the enthalpy calculations are well converged to better than 1 meV/atom. Phonon dispersion and electron-phonon coupling calculations were performed with density functional perturbation theory using the Quantum-ESPRESSO⁴³ package with kinetic energy cutoffs of 80 Ry, $2 \times 2 \times 2$ and $2 \times 2 \times 1$ q -meshes in the first Brillouin zones were used in the electron-phonon coupling calculations for Ca_2Sb and Sc_2As , respectively.

References

1. Walsh, A. & Scanlon, D. O. Electron excess in alkaline earth sub-nitrides: 2D electron gas or 3D electride? *J. Mater. Chem. C* **1**, 3525 (2013).
2. Dye, J. L. Physical and chemical properties of alkalides and electrides. *Annu. Rev. Phys. Chem.* **38**, 271–301 (1987).
3. Redko, M. Y., Jackson, J. E., Huang, R. H. & Dye, J. L. Design and synthesis of a thermally stable organic electride. *J. Am. Chem. Soc.* **127**, 12416–12422 (2005).
4. Ichimura, A. S., Dye, J. L., Cambor, M. a. & Villaescusa, L. a. Toward inorganic electrides. *J. Am. Chem. Soc.* **124**, 1170–1171 (2002).
5. Dye, J. L. Electrides: early examples of quantum confinement. *Acc. Chem. Res.* **42**, 1564–1572 (2009).
6. Dawes, S. B., Ward, D. L., Huang, R. H. & Dye, J. L. First electride crystal structure. *J. Am. Chem. Soc.* **108**, 3534–3535 (1986).
7. Phillips, R. C., Pratt, W. P. & Dye, J. L. Thermionic emission from cold electride films. *Chem. Mater.* **12**, 3642–3647 (2000).
8. Matsuishi, S. *et al.* High-density electron anions in a nanoporous single crystal: $[\text{Ca}_{24}\text{Al}_{28}\text{O}_{64}]^{4+} (4e^-)$. *Science* **301**, 626–629 (2003).
9. Toda, Y. *et al.* Field emission of electron anions clathrated in subnanometer-sized cages in $[\text{Ca}_{24}\text{Al}_{28}\text{O}_{64}]^{4+} (4e^-)$. *Adv. Mater.* **16**, 685–689 (2004).
10. TSAI, M., Seip, U., Bassignana, I. C., Kuppers, J. & Ertl, G. A vibrational spectroscopy study on the interaction of N_2 with clean and K-promoted Fe(111) surfaces: pi-bonded dinitrogen as precursor for dissociation. *Surf. Sci.* **155**, 387–399 (1985).
11. Kitano, M. *et al.* Ammonia synthesis using a stable electride as an electron donor and reversible hydrogen store. *Nat. Chem.* **4**, 934–940 (2012).
12. Lee, K., Kim, S. W., Toda, Y., Matsuishi, S. & Hosono, H. Dicalcium nitride as a two-dimensional electride with an anionic electron layer. *Nature* **494**, 336–40 (2013).
13. Kim, Y. J. *et al.* Two-dimensional inorganic electride-promoted electron transfer efficiency in transfer hydrogenation of alkynes and alkenes. *Chem. Sci.* **6**, 3577–3581 (2015).
14. Zhao, S., Li, Z. & Yang, J. Obtaining Two-Dimensional Electron Gas in Free Space without Resorting to Electron Doping: An Electride Based Design. *J. Am. Chem. Soc.* **136**, 13313–13318 (2014).
15. Ma, Y. *et al.* Transparent dense sodium. *Nature* **458**, 182–185 (2009).
16. Lv, J., Wang, Y., Zhu, L. & Ma, Y. Predicted novel high-pressure phases of lithium. *Phys. Rev. Lett.* **106**, 19–22 (2011).
17. Li, P., Gao, G., Wang, Y. & Ma, Y. Crystal structures and exotic behavior of magnesium under pressure. *J. Phys. Chem. C* **114**, 21745–21749 (2010).
18. Pickard, C. J. & Needs, R. J. Aluminium at terapascal pressures. *Nat. Mater.* **9**, 624–627 (2010).
19. Oganov, A. R. *et al.* Exotic behavior and crystal structures of calcium under pressure. *Proc. Natl. Acad. Sci. U. S. A.* **107**, 7646–7651 (2010).
20. Miao, M. & Hoffmann, R. High pressure electrides: A predictive chemical and physical theory. *Acc. Chem. Res.* **47**, 1311–1317 (2014).
21. Tada, T., Takemoto, S., Matsuishi, S. & Hosono, H. High-throughput ab initio screening for two-dimensional electride materials. *Inorg. Chem.* **53**, 10347–10358 (2014).

22. Zhang, X. *et al.* Two-dimensional transition-metal electride Y_2C . *Chem. Mater.* **26**, 6638–6643 (2014).
23. Wang, Y., Lv, J., Zhu, L. & Ma, Y. Crystal structure prediction via particle-swarm optimization. *Phys. Rev. B - Condens. Matter Mater. Phys.* **82**, 1–8 (2010).
24. Wang, Y., Lv, J., Zhu, L. & Ma, Y. CALYPSO: A method for crystal structure prediction. *Comput. Phys. Commun.* **183**, 2063–2070 (2012).
25. Wang, Y. & Ma, Y. Perspective: Crystal structure prediction at high pressures. *J. Chem. Phys.* **140**, 040901 (2014).
26. Zhang, X. *et al.* First-principles structural design of superhard materials. *J. Chem. Phys.* **138**, (2013).
27. Becke, A. D. & Edgecombe, K. E. A simple measure of electron localization in atomic and molecular systems. *J. Chem. Phys.* **92**, 5397 (1990).
28. Savin, A., Nesper, R., Wengert, S. & Fassler, T. E. ELF : The electron localization function. *Angew. Chemie Int. Ed. English* **36**, 1808–1832 (1997).
29. Burdett, J. K. & McCormick, T. a. Electron localization in molecules and solids: the meaning of ELF. *J. Phys. Chem. A* **102**, 6366–6372 (1998).
30. Lv, J. *et al.* Particle-swarm structure prediction on clusters Particle-swarm structure prediction on clusters. **084104**, (2012).
31. Pauling, C. L. *The Nature of the Chemical Bond* (Cornell Univ. Press, Ithaca, New York, 1960).
32. Xu, Y., Yamazaki, M. & Villars, P. Inorganic materials database for exploring the nature of material. *Jpn. J. Appl. Phys.* **50**, 11RH02 (2011).
33. Gražulis, S. *et al.* Crystallography Open Database (COD): an open-access collection of crystal structures and platform for world-wide collaboration. *Nucleic Acids Res.* **40**, 420–427 (2012).
34. M., S. Die Krystalstruktur des CaC_2 . *Naturwissenschaften* **18**, 305–306 (1930).
35. Heyd, J., Scuseria, G. E. & Ernzerhof, M. Hybrid functionals based on a screened Coulomb potential. *J. Chem. Phys.* **118**, 8207–8215 (2003).
36. Krukau, A. V., Vydrov, O. a., Izmaylov, A. F. & Scuseria, G. E. Influence of the exchange screening parameter on the performance of screened hybrid functionals. *J. Chem. Phys.* **125**, 224106 (2006).
37. Araujo, R. E. & Corbett, J. D. Lanthanum monochloride and lanthanum sesquichloride. *Inorg. Chem.* **20**, 3082–3086 (1981).
38. Miyakawa, M. *et al.* Superconductivity in an inorganic electride $12CaO \cdot 7Al_2O_3:e^-$. *J. Am. Chem. Soc.* **129**, 7270–7271 (2007).
39. Hosono, H. *et al.* Superconductivity in room-temperature stable electride and high-pressure phases of alkali metals. *Phil. Trans. R. Soc.A* **373**, 20140450 (2015).
40. Kresse, G. & Furthmüller, J. Efficiency of ab-initio total energy calculations for metals and semiconductors using a plane-wave basis set. *Comput. Mater. Sci.* **6**, 15–50 (1996).
41. Kresse, G. From ultrasoft pseudopotentials to the projector augmented-wave method. *Phys. Rev. B* **59**, 1758–1775 (1999).
42. Heyd, J., Peralta, J. E., Scuseria, G. E. & Martin, R. L. Energy band gaps and lattice parameters evaluated with the Heyd-Scuseria-Ernzerhof screened hybrid functional. *J. Chem. Phys.* **123**, 174101 (2005).
43. Scandolo, S. *et al.* First-principles codes for computational crystallography in the

Author Contributions:

Y. M. designed the research. Y. Z. performed most of the calculations. Y. Z., H. W., and Y. W. coded the inverse design method into CALYPSO. Y. Z. and Y. M. analyzed the results and wrote the manuscript. All authors commented on the manuscript.

Acknowledgements

The authors acknowledge support from National Natural Science Foundation of China under Grants

No.11274136 and No.11534003, 2012 Changjiang Scholar of Ministry of Education. L.Z. acknowledges funding support from the Recruitment Program of Global Experts (the Thousand Young Talents Plan).

Competing financial interests

The authors declare no competing financial interests.

(b) Illustration of the V_{inter} in a crystal. The interstitial regions where electron localized well (V_{inter}) are where the ELF value larger than 0.75 in ELF map. As an illustration, V_{inter} are yellow parts circled by green dashed lines in (b).

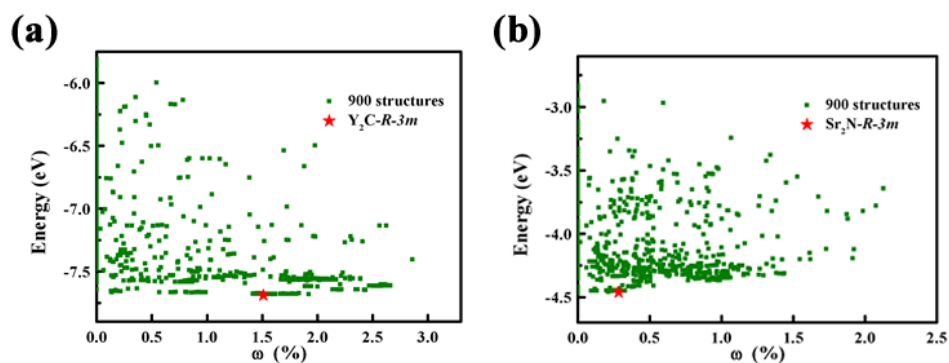


Figure S2. ω (%) vs. energy maps of Sr_2N (a) and Y_2C (b), respectively. Green squares are 900 structures produced by CALYPSO code with 30 generations for each system. The desirable $R3m$ electricle structures for Sr_2N and Y_2C are shown as red stars.

Formula	Z	Space Group	Prototype structure	a (Å)	b (Å)	c (Å)	ω	E_{diff}	C_{ref}
Be_2C									
Be_2N	6	$R3m$	Be_2N	2.8065	2.8065	19.8461	3.27E-02	0.1885	Be_3N_2 , Be(s)
Be_2As	6	$R3m$	Be_2As	4.2070	4.2070	16.5828	9.42E-03	-0.0611	As(s), Be(s)
Be_2Sb	6	$P3m1$	Be_2Sb	4.2939	4.2939	7.4351	1.29E-02	0.0768	Sb(s), Be(s)
Be_2Bi	6	$R-3m$	Be_2Bi	3.4688	3.4688	30.2381	1.60E-02	0.0174	Bi(s), Be(s)
Be_2O	6	$R3m$	Be_2N	2.6114	2.6114	24.7554	5.66E-02	0.269	BeO, Be(s)
Be_2S									
BeCl	4	$R-3m$	ZrCl	3.1396	3.1396	25.7290	3.61E-02	0.508	BeCl, Be(s)
BeBr									
Mg_2C									
Mg_2N	6	$Cmcm$	Mg_2N	3.2606	14.2928	4.0728	7.14E-02	0.105	Mg_3N_2 , Mg(s)
Mg_2As	6	$I4/mmm$	La_2Sb	4.1334	4.1334	14.0811	1.25E-02	0.077	Mg_3As_2 , Mg(s)
Mg_2Sb	3	$Cmmm$	ThH_2	12.9459	3.4534	3.4606	5.65E-02	0.1313	Mg_3Sb_2 , Mg(s)
Mg_2Bi	6	$Immm$	Te_2U	13.3562	6.3702	3.6953	1.24E-02	0.060175	Mg_3Bi_2 , Mg(s)
Mg_2O	6	$P-3m1$	Mg_2O	3.0736	3.0736	10.0092	1.37E-02	0.1452	MgO, Mg(s)
Mg_2S	3	$P-3m1$	CdI_2	3.6183	3.6183	3.6183	8.28E-02	0.138	MgS, Mg(s)
MgCl	4	$R-3m$	ZrCl	3.6387	3.6387	27.4723	5.37E-02	0.149	MgCl_2 , Mg(s)
MgBr	4	$R-3m$	ZrCl	3.7788	3.7788	29.4562	5.66E-02	0.148	MgBr_2 , Mg(s)
Ca_2C	6	$P4/mmm$	Ca_2C	3.7592	3.7592	12.1695	2.63E-02	-0.00223	CaC_2 , Mg(s)
Ca_2N^*	3	$R-3m$	CdCl_2	3.6093	3.6093	19.2631	2.78E-03	0.09942	Ca_3N_2 , Ca(s)
Ca_2As^*	6	$I4/mmm$	La_2Sb	4.5992	4.5992	15.9292	4.05E-02	0.0436	Ca_5As_3 , Ca(s)

Ca ₂ Sb*	6	<i>I4/mmm</i>	La ₂ Sb	4.8060	4.8060	16.8108	0.1525753	-0.0174	Ca ₅ Sb ₃ , Ca(s)
Ca ₂ Bi*	6	<i>I4/mmm</i>	La ₂ Sb	4.8902	4.8902	17.0871	3.68E-02	-0.0194	Ca ₅ Bi ₃ , Ca(s)
Ca ₂ O	6	<i>R-3m</i>	Be ₂ N	3.5669	3.5669	36.4600	4.59E-02	0.113	CaO, Ca(s)
Ca ₂ S	6	<i>R-3m</i>	Be ₂ N	4.0084	4.0084	39.3227	8.70E-02	0.056708	CaS, Ca(s)
CaCl	4	<i>R-3m</i>	ZrCl	4.0676	4.0676	31.1211	7.58E-02	0.09714	CaCl ₂ , Ca(s)
CaBr	4	<i>R-3m</i>	ZrCl	4.2287	4.2287	31.4769	6.22E-02	0.111	CaBr ₂ , Ca(s)
Sr ₂ C	6	<i>P4/mmm</i>	Ca ₂ C	4.0603	4.0603	13.0583	6.47E-03	0.04215	SrC ₂ , Sr(s)
Sr ₂ N*	3	<i>R-3m</i>	CdCl ₂	3.8617	3.8617	20.8583	1.36E-03	-0.291	SrN ₂ , Sr(s)
Sr ₂ As*	6	<i>I4/mmm</i>	La ₂ Sb	4.8662	4.8662	16.9452	9.90E-03	0.0735	Sr ₅ As ₃ , Sr(s)
Sr ₂ Sb*	6	<i>I4/mmm</i>	La ₂ Sb	5.0579	5.0579	17.8723	1.23E-02	0.0219	Sr ₅ Sb ₃ , Sr(s)
Sr ₂ Bi*	6	<i>I4/mmm</i>	La ₂ Sb	5.1512	5.1512	18.1609	1.22E-02	0.0179	Sr ₅ Bi ₃ , Sr(s)
Sr ₂ O	6	<i>R-3m</i>	Be ₂ N	3.5669	3.5669	36.4601	5.87E-02	0.12945	SrO, Sr(s)
Sr ₂ S	6	<i>P4/nmm</i>	HgI ₂	4.2936	4.2936	12.0230	3.00E-02	0.0688	SrS, Sr(s)
SrCl	6	<i>P4/nmm</i>	PbO	4.8790	4.8790	6.7727	2.66E-02	0.264	SrCl ₂ , Sr(s)
SrBr	6	<i>P4/nmm</i>	SrBr	4.2159	4.2159	8.3054	2.03E-02	0.1195	SrBr ₂ , Sr(s)
Ba ₂ C	6	<i>P4/mmm</i>	Ca ₂ C	4.318	4.318	13.8603	3.16E-03	0.0387	BaC ₂ , Ba(s)
Ba ₂ N*	3	<i>R-3m</i>	CdCl ₂	4.0573	4.0573	22.8424	3.17E-03	0.00273	Ba ₃ N, Ba(s)
Ba ₂ As	6	<i>I4/mmm</i>	La ₂ Sb	5.0932	5.0932	18.0885	6.65E-03	0.115	Ba ₅ As ₃ , Ba(s)
Ba ₂ Sb*	6	<i>I4/mmm</i>	La ₂ Sb	5.2865	5.2865	19.0667	1.74E-03	0.02277	Ba ₅ Sb ₃ , Ba(s)
Ba ₂ Bi*	6	<i>I4/mmm</i>	La ₂ Sb	5.3733	5.3733	19.3419	2.11E-03	0.01833	Ba ₅ Bi ₃ , Ba(s)
Ba ₂ O	6	<i>P4/nmm</i>	Cu ₂ Sb	5.1875	5.1875	9.4619	4.34E-02	0.05275	BaO, Ba(s)
Ba ₂ S	6	<i>P4/nmm</i>	HgI ₂	4.5648	4.5648	12.7880	7.19E-03	0.068	BaS, Ba(s)
BaCl	4	<i>R-3m</i>	CuI	5.0894	5.0894	25.4030	2.09E-02	0.1075	BaCl ₂ , Ba(s)
BaBr	6	<i>R-3m</i>	CuI	5.2051	5.2051	27.483	6.73E-03	0.105	BaBr ₂ , Ba(s)
Sc ₂ C	3	<i>R-3m</i>	CdCl ₂	3.3228	3.3228	16.5998	3.48E-02	-0.0799	Sc ₄ C ₃ , Sc(s)
Sc ₂ N	3	<i>R-3m</i>	CdCl ₂	3.2182	3.2182	15.9749	4.58E-02	-0.01	ScN, Sc(s)
Sc ₂ As	6	<i>P4/nmm</i>	Cu ₂ Sb	3.9785	3.9785	7.4978	1.73E-02	0.0045	Sc ₅ As ₃ , Sc(s)
Sc ₂ Sb*	6	<i>P4/nmm</i>	Cu ₂ Sb	4.2110	4.2110	7.8140	1.21E-02	-0.02	Sc ₅ Sb ₃ , Sc(s)
Sc ₂ Bi	6	<i>P4/nmm</i>	Cu ₂ Sb	4.2949	4.2949	7.9737	1.29E-02	-0.103	ScBi, Sc(s)
Sc ₂ O	6	<i>I4₁</i>	TiN ₂	4.3774	4.3774	9.6834	7.91E-03	-0.0482	Sc ₂ O ₃ , Sc(s)
Sc ₂ S	6	<i>P4/nmm</i>	HgI ₂	3.6395	3.6395	9.2827	1.19E-02	0.02004	ScS, Sc(s)
ScCl	4	<i>R-3m</i>	ZrCl	3.5188	3.5188	30.2238	2.31E-02	0.0084	ScCl ₃ , Sc(s)
ScBr	4	<i>P-3m1</i>	ScBr	3.6156	3.6156	10.4459	1.74E-02	0.0454	ScBr ₃ , Sc(s)
Y ₂ C*	3	<i>R-3m</i>	CdCl ₂	3.6117	3.6116	18.4237	1.85E-02	-0.0961	Y ₄ C ₅ , Y(s)
Y ₂ N	3	<i>R-3m</i>	CdCl ₂	3.5219	3.5219	17.6952	2.73E-02	0.0503	YN, Y(s)
Y ₂ As	6	<i>Immm</i>	Y ₂ As	13.0474	3.9671	6.0464	8.19E-03	0.0948	YAs, Y(s)
Y ₂ Sb	6	<i>P4/nmm</i>	Cu ₂ Sb	4.4971	4.4971	8.4669	7.95E-03	0.0223	Y ₅ Sb ₃ , Y(s)
Y ₂ Bi	6	<i>P4/nmm</i>	Cu ₂ Sb	4.5754	4.5754	8.6188	8.40E-03	0.0113	Y ₅ Bi ₃ , Y(s)
Y ₂ O	6	<i>P4₂/nmc</i>	HgI ₂	3.7612	3.7612	10.6135	4.14E-03	0.0825	Y ₂ O ₃ , Y(s)
Y ₂ S	6	<i>P4/nmm</i>	Y ₂ S	3.9125	3.9125	10.1780	2.72E-03	0.0109	YS, Y(s)
YCl*	4	<i>R-3m</i>	ZrCl	3.7308	3.7308	46.1839	9.36E-03	0.071	YCl ₃ , Y(s)
YBr*	4	<i>P-3m1</i>	ScBr	3.8080	3.8080	14.6172	5.67E-03	0.0626	Y ₂ Br ₃ , Y(s)
La ₂ C	3	<i>P-3m1</i>	La ₂ C	3.7269	3.7269	6.9088	7.63E-04	-0.03283	La ₂ C ₃ , La(s)

La ₂ N	3	<i>R-3m</i>	CdCl ₂	3.6793	3.6793	20.3756	5.08E-03	-0.00317	LaN, La(s)
La ₂ As	6	<i>P6₃/mmc</i>	MoS ₂	4.2359	4.2359	13.5345	1.48E-02	0.305	La ₄ As ₃ , La(s)
La ₂ Sb	6	<i>P4/nmm</i>	Cu ₂ Sb	4.6811	4.6811	9.1226	1.89E-03	-0.019	LaSb, La(s)
La ₂ Bi	3	<i>R-3m</i>	CdCl ₂	4.4640	4.4640	21.1735	2.16E-03	0.281	La ₅ Bi ₃ , La(s)
La ₂ O	3	<i>R-3m</i>	CdI ₂	3.7951	3.7951	6.2679	6.29E-03	0.1811	LaO, La(s)
La ₂ S	6	<i>R3m</i>	La ₂ S	3.9462	3.9462	40.6260	7.92E-02	0.0755	LaS, La(s)
LaCl*	4	<i>R-3m</i>	ZrCl	4.0654	4.0654	30.3248	9.73E-03	0.055	LaCl ₃ , La(s)
LaBr*	4	<i>R-3m</i>	ZrCl	4.1333	4.1333	29.7150	9.01E-03	0.1015	LaBr ₂ , La(s)
Zr ₂ C	3	<i>R-3m</i>	CdCl ₂	3.3478	3.3478	16.1704	9.51E-03	-0.057	ZrC, Zr(s)
Zr ₂ N	3	<i>R-3m1</i>	CdI ₂	3.2919	3.2919	5.2698	6.86E-03	-0.0504	ZrN, Zr(s)
Zr ₂ As	3	<i>I4/mmm</i>	MoSi ₂	3.5674	3.5674	9.5248	2.11E-02	0.354	Zr ₃ As ₂ , Zr(s)
Zr ₂ Sb	4	<i>I4/mmm</i>	MoSi ₂	3.7492	3.7492	9.6087	1.46E-02	0.0481	Zr ₅ Sb ₃ , Zr(s)
Zr ₂ Bi	4	<i>I4/mmm</i>	MoSi ₂	3.8123	3.8123	9.7705	1.43E-02	-0.0377	ZrBi, Zr(s)
Zr ₂ O	6	<i>Pnmm</i>	FeS ₂	5.1766	5.1766	3.2179	1.30E-02	-0.3018	ZrO, Zr(s)
Zr ₂ S*	3	<i>P-3m1</i>	CdI ₂	3.5384	3.5384	5.6365	2.00E-02	-0.175	ZrS, Zr(s)
ZrCl*	4	<i>R-3m</i>	ZrCl	3.4272	3.4272	30.3364	2.26E-02	-0.133	ZrCl ₃ , Zr(s)
ZrBr*	4	<i>R-3m</i>	ZrCl	3.5258	3.5258	31.5407	1.96E-02	-0.0757	ZrBr ₃ , Zr(s)
Hf ₂ C	3	<i>R-3m</i>	CdCl ₂	3.2869	3.2869	15.7881	4.55E-03	-0.094	HfC, Hf(s)
Hf ₂ N	3	<i>P-3m1</i>	CdI ₂	3.2333	3.2333	5.1616	1.60E-02	-0.1358	HfN, Hf(s)
Hf ₂ As	6	<i>Immm</i>	Te ₂ U	3.4908	5.6141	12.1631	1.00E-02	0.0281	Hf ₃ As ₂ , Hf(s)
Hf ₂ Sb	3	<i>I4/mmm</i>	MoSi ₂	3.6988	3.6988	9.5574	1.75E-02	-0.00421	Hf ₅ Sb ₃ , Hf(s)
Hf ₂ Bi	3	<i>I4/mmm</i>	MoSi ₂	3.7547	3.7547	9.7950	1.64E-02	-0.06017	HfBi, Hf(s)
Hf ₂ O	3	<i>P-3m1</i>	CdI ₂	3.2187	3.2187	5.1306	4.28E-02	-0.13738	HfO ₂ , Hf(s)
Hf ₂ S*	6	<i>P6₃/mmc</i>	NbS ₂	3.3748	3.3748	11.7720	3.20E-02	-0.3333	HfS ₂ , Hf(s)
HfCl*	4	<i>R-3m</i>	ZrCl	3.3704	3.3704	29.6932	2.50E-02	-0.1578	HfCl ₄ , Hf(s)
HfBr*	4	<i>R-3m</i>	ZrCl	3.5067	3.5067	31.6268	2.26E-02	-0.112	HfBr ₄ , Hf(s)
Al ₂ C	3	<i>P-3m1</i>	CdI ₂	3.1047	3.1047	4.4460	3.64E-02	0.0709	Al ₄ C ₃ , Al(s)
Al ₂ N	6	<i>I-4m2</i>	Al ₂ N	3.117	3.117	17.1591	8.71E-02	0.0826	AlN, Al(s)
Al ₂ As	6	<i>I-4m2</i>	Al ₂ N	3.9138	3.9138	19.3565	5.75E-02	0.229	AlAs, Al(s)
Al ₂ Sb	6	<i>I-4m2</i>	Al ₂ N	4.2602	4.2602	19.6040	6.82E-02	0.275	AlSb, Al(s)
Al ₂ Bi									
Al ₂ O	2	<i>R3m</i>	Al ₂ O	2.8912	2.8912	10.4176	1.94 E-03	0.131	Al ₂ O ₃ , Al(s)
Al ₂ S	6	<i>P-3m1</i>	Al ₂ S	3.3924	3.3924	12.9981	3.05E-02	0.165	Al ₂ S ₃ , Al(s)
AlCl	4	<i>Pmnm</i>	AlCl	3.1735	3.5344	8.6712	3.19E-02	0.24	AlCl ₃ , Al(s)
AlBr									

Table S2. Prototype structure, relaxed lattice data, degree of interstitial electron localization, and formation energy with respect to existing compounds of all designed binary electriles. a, b, and c are crystal lattice parameters of their unit cell, respectively. ω is the degree of interstitial electron localization. E_{diff} is the formation energy with respect to the existing stable compounds (C_{ref}). Compounds with asterisk (*) have already been synthesized.

Elements	Ratio (%)						
Li ₄ N	83.1	Tl ₂ N	0.0	Hf ₂ N	29.2	Co ₂ N	0.0
Na ₄ N	62.2	Ge ₂ N	0.0	V ₂ N	0.6	Rh ₂ N	0.0
K ₄ N	23.1	Sn ₂ N	0.0	Nb ₂ N	0.6	Ir ₂ N	0.0
Rb ₄ N	15.6	Pb ₂ N	0.0	Ta ₂ N	15.6	Ni ₂ N	0.0
Cs ₄ N	2.3	Sb ₂ N	0.0	Cr ₂ N	3.3	Pd ₂ N	0.0
Be ₂ N	74.1	Bi ₂ N	0.0	Mo ₂ N	0.2	Pt ₂ N	0.0
Mg ₂ N	51.8	Po ₂ N	0.0	W ₂ N	0.2	Cu ₂ N	0.0
Ca ₂ N	87.7	Sc ₂ N	87.6	Mn ₂ N	0.0	Ag ₂ N	0.0
Sr ₂ N	65.1	Y ₂ N	71.5	Tc ₂ N	0.0	Au ₂ N	0.0
Ba ₂ N	37.7	La ₂ N	20.2	Re ₂ N	0.0	Zn ₂ N	0.0
Al ₂ N	87.5	Ac ₂ N	1.8	Fe ₂ N	1.3	Cd ₂ N	0.0
Ga ₂ N	0.2	Ti ₂ N	3.5	Ru ₂ N	0.0	Hg ₂ N	0.0
In ₂ N	0.0	Zr ₂ N	13.8	Os ₂ N	0.0		

Table S3. Chemical stoichiometries of nitrides in the model system of metal nitrides and the ratios of electrone structures over all structures generated by CALYPSO code (formation probability of electrone structures).

Prototype	Space group	Z	Wyckoff position
Be ₂ N	<i>R3m</i>	6	Be1: 3a (0, 0, 5885), Be4: 3a (0, 0, 0.1679) Be7: 3a (0, 0, 4234), Be10: 3a (0, 0, 0) N13: 3a (0, 0, 0.2931), N16: 3a (0, 0, 0.0844)
Be ₂ As	<i>R3m</i>	6	Be1: 3a (0, 0, -0.4342), Be2: 9b (0.1648, -0.1648, -0.3145) As5: 3a (0, 0, -0.0967), As6: 3a (0, 0, -0.5794)
Be ₂ Sb	<i>P3m1</i>	2	Be1: 3d (0.4983, -0.0035, 0.1496), Be2: 1b (0.3333, 0.6667, 0.8994) Sb5: 1c(0.6667, 0.3333, 0.8493), Sb6: 1a(0, 0, 0.3388)
Mg ₂ N	<i>Cmcm</i>	4	Mg1: 4c(1, -0.0857, 0.25), Mg3: 4c(0.5, 0.2165, 0.25) N5: 4c(0.5, 0.1815, 0.75)
Mg ₂ O	<i>P-3m1</i>	2	Mg1: 2d(0.3333, 0.6667, 0.2546), Mg2: 1b(0, 0, 0.5) Mg3: 1a(0, 0, 0) O5: 2d(0.6667, 0.3333, 0.3790)
Ca ₂ C	<i>P4/mmm</i>	2	Ca1: 2f (0, 0, 0.5), Ca2: 2h (0.5, 0.5, 0.7457) Ca3: 2h (0.5, 0.5, 0.2543), Ca4: 1a (1, 1, 1) C1: 2h (0.5, 0.5, 0.0537), C2: 2h (0.5, 0.5, 0.9463)
SrBr	<i>P4/nmm</i>	2	Sr1: 2c(0, 0.5, 0.7068) Br3: 2c(0, 0.5, 0.1370)
ScBr	<i>P-3m1</i>	2	Sc1: 2d(0.3333, 0.6667, 0.8799) Br3: 2c(0, 0, 0.2879)
Y ₂ As	<i>Immm</i>	4	Y1: 4j(0, 0.5, 0.3007), Y2: 4g(0, 0.2601, 0)

			As9: 4i(0, 0, 0.6413)
Y ₂ S	<i>P4/nmm</i>	2	Y1: 2c(0.5, 0, 0.6035), Y3: 2c(0.5, 0, 0.1404) S5: 2c(0.5, 0, 0.8735)
La ₂ C	<i>P-3m1</i>	1	La1: 2d(-0.3333, -0.6667, 0.2092) C5: 1a(0, 0, 0)
La ₂ S	<i>R3m</i>	6	La1: 3a(0, 0, 0.2686), La2: 3a(0, 0, 0.1162), La3: 3a(0, 0, 0.6923), La4: 3a(0, 0, 0.8594) S5: 3a(0, 0, 0.4032), S6: (0, 0, 0.9813)
Al ₂ N	<i>I-4m2</i>	4	Al1: 4f(0.5, 0, 0.6221), Al2: 2a(0.5, 0.5, 0.5), Al5: 2d(0, 0.5, 0.75) N9: 4e(0.5, 0.5, 0.8137)
Al ₂ O	<i>R-3m</i>	6	Al1: 3b(0, 0, 0.5), Al2: (0, 0, 0) Al3: 6c(0, 0, 0.7610) O5: 6c(0, 0, 0.3020)
Al ₂ S	<i>P-3m1</i>	2	Al1: 2d(0.6667, 0.3333, 0.0767), Al2: (0, 0, 0.7548) S5: 2d(0.6667, 0.3333, 0.6641)
AlCl	<i>Pmmn</i>	2	Al1: 2a(0, 0, 0.5859) Cl3: 2b(0.5, 0, 0.7849)

Table S4. Structural information of 16 new prototype structures.